Journal of Alloys and Compounds, 194 (1993) 23–30
JALCOM 542

Far-from-equilibrium phase transition induced by mechanical alloying in the Cu–Fe system

E. Gaffet, M. Harmelin and F. Faudot
Centre d'Etudes de Chimie Métallurgique, CNRS, 15 Rue G. Urbain, F-94407 Vitry sur Seine Cedex (France)

(Received September 1, 1992)

Abstract

By means of X-ray diffraction patterns, scanning electron microscopy observations, chemical energy-dispersive analyses and thermal stability studies (differential scanning calorimetry and thermomagnetometry), the far-from-equilibrium phase transition induced by mechanical alloying in the Fe–Cu system has been investigated. On the Cu-rich side of the phase diagram a supersaturated f.c.c. crystalline (Cu) solid solution is detected, while on the Fe-rich side a supersaturated b.c.c. (Fe) solid solution is detected. The sticking of the Cu particles which occurs during milling (leading to a Cu end-product depletion) is avoided by the addition of an ethanol fluid to the initial Fe and Cu powder mixture, resulting in a better homogenization of the end-product (in terms of composition). In this case an amorphous phase has been found in addition to the former supersaturated crystalline phases.

1. Introduction

The far-from-equilibrium phase transition induced by ball milling (BM) or mechanical alloying (MA) was first reported by Yermakov *et al.* [1] and Koch *et al.* [2] for the Co–Y and Ni–Nb binary systems respectively. Such a phase transition was assumed to require some prerequisite conditions: a negative heat of mixing and the presence of a fast diffuser. Nevertheless, amorphization induced by MA was reported for a system exhibiting no fast diffuser: V–Zr [3]. Recently the crystal-to-amorphous phase transition was obtained for binary systems exhibiting a positive heat of mixing: Si–Sn, Si–Zn [4], Cu–Ta [5], Cu–V [6], Cu–W [7] and Cu–Fe (see below). BM amorphization was also reported in the case of the phase exhibiting a diamond cubic structure: Si [8], Ge [9], Ge_xSi_{1-x} [10] and GaAs [11].

From a practical point of view the MA of Cu with insoluble elemental additions is a potential way to produce high strength alloys maintaining high electrical and thermal conductivity [12].

From a fundamental viewpoint the Cu–Fe binary equilibrium system exhibits an insolubility from room temperature up to 600 °C. Supersaturated b.c.c. (Fe) (up to 30 at.% Cu) and f.c.c. (Cu) (up to 60 at.% Fe) solid solutions were claimed to be obtained [13–16] by mechanical alloying, but the milling machines (a planetary machine [13, 14] and a vibrating one [15, 16]) are not described well in these papers.

In this paper, using a well-defined high energy planetary milling machine [17, 18], the MA formation of metastable supersaturated b.c.c. (Fe) and f.c.c. (Cu) phases is reported. The influence of a solvent addition (here ethanol) on the expansion of such metastable end-product domains is discussed.

2. Experimental details and results

2.1. Mechanical alloying conditions

Pure Fe and Cu powders (10 g) were introduced into a cylindrical tempered steel container of capacity 45 ml. This procedure was performed in a glove-box filled with purified argon. Each container was loaded with five balls (diameter 1.5 cm, mass 14 g). The containers were sealed in a glove-box with a Teflon O-ring and the milling thus proceeded in a stationary argon atmosphere.

In the experiments in which an ethanol volume corresponding to 1 cm^3 had been added, the filling procedure was performed in an air atmosphere. As above, the containers were then sealed with an O-ring to avoid air input during the process duration. In other words, the milling set-up comprises 10 g of powder, 1 cm^3 of ethanol and less than 45 ml of air atmosphere.

MA was carried out using the so-called "G5" high energy planetary ball-milling machine, which allows independent choice of the shock frequency and shock energy. Such a milling machine has been designed and

0925-8388/93/$6.00

realized at CECM/CNRS. The MA conditions were $\Omega = 305$ rev min^{-1}, $\omega = 675$ rev min^{-1} and $\Delta t = 240$ h, where Ω is the rotation speed of the disc on which the vial holders are fixed. The latter turn at a rotation speed ω. The duration of the process was Δt. Such a long duration has been estimated to yield the steady state end-product. An electronic tachometer controls the effective rotation speeds during milling.

2.2. Scanning electron microscopy and chemical energy-dispersive analyses

Some MA (Fe–Cu) particles were taken from the vial for further electron microscopy investigations: the particle morphology (see Fig. 1) was characterized using a digital scanning electron microscope (Zeiss DSM 950) in the secondary electron image mode. The MA end-product corresponds to a mixture of 50–100 μm grains exhibiting a very ductile fracture surface with typical dimples of about 100 nm. Such a surface morphology has been found in the case of Ni–Zr milled powder [19]. In order to evaluate the possible container contamination which may have occurred by friction of the particles on the balls and on the walls of the containers, energy-dispersive X-ray (EDX) analyses on large surfaces (in the scanning mode) were performed using an Si–Li detector and a Tracor EDX analyser in conjunction with the scanning electron microscope. A semiquantitative programme was used to analyse the EDX spectra. The EDX results are listed in Tables 1 and 2.

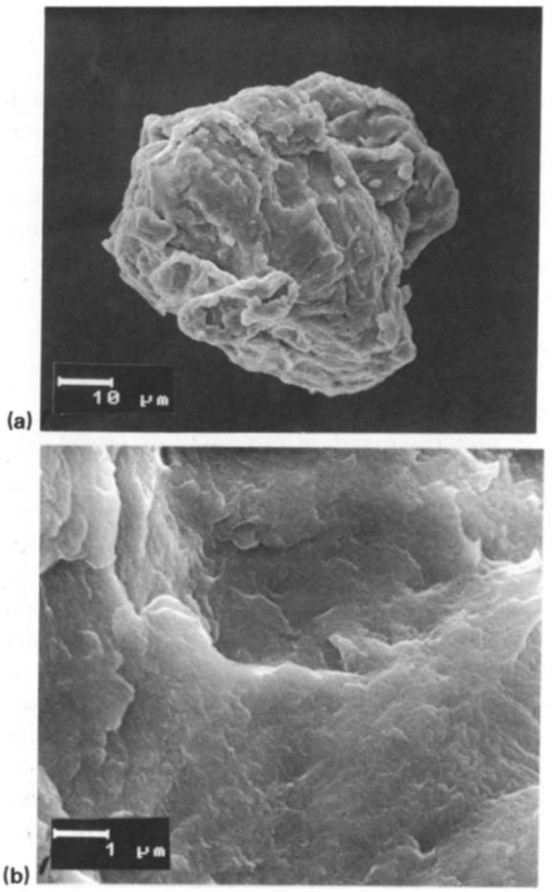

Fig. 1. Typical scanning electron micrographs (secondary electron image mode) corresponding to a dry mechanically milled powder (initial composition 80 wt.% Fe). The lower micrograph details the surface of the powder (with typical ductile fracture dimples of about 100 nm) exhibited in the upper one.

2.3. X-Ray diffraction pattern investigations

After continuous milling, a small amount of MA powder was extracted from the container and glued onto a silica plate for X-ray diffraction (XRD) investigations. The XRD patterns were obtained using a θ–2θ Philips diffractometer with Co Kα radiation of wavelength $\lambda = 0.17889$ nm.

Figure 2(a) shows the XRD patterns corresponding to the milling process without any solvent addition, while Figs. 2(b) and 2(c) show the XRD patterns corresponding to the milling process with ethanol addition. On Fig. 2(c) the XRD peaks corresponding to the additional phases Fe_3O_4 and Fe_3C are indicated.

Two numerical methods were used to analyse the XRD patterns and to obtain the position and full width at half-height of the various peaks:

(1) the ABFfit method [20] using a deconvolution based on the gaussian peak shapes (for details of such an application of the numerical method, see our previous work on the amorphization of silicon by ball milling [8]);

(2) the Automated Powder Diffraction numerical method (developed by Philips and hereafter called the APD method), which is well adapted in the case of well-defined crystalline XRD peaks but not when superimposed on a minor amorphous halo [10], which is the reason why both methods were used.

The b.c.c. (Fe) and f.c.c. (Cu) phase lattice parameters were calculated by taking into account the first three crystalline peaks of each phase, *i.e.* the [110], [200] and [211] crystalline XRD peaks for the b.c.c. phase and the [111], [200] and [220] crystalline XRD peaks for the f.c.c. phase. The lattice parameters are shown in Figs. 3(a) and 3(b) and the relative changes in the MA lattice parameters are given in Tables 1 and 2 (Δ expressed as a percentage).

The Scherrer formula was used to estimate the crystallite size, which is hereafter denoted Φ:

$$\Phi = \frac{0.9\,\lambda}{\Delta(2\theta)\cos\theta}$$

where λ is the X-ray wavelength, $\Delta(2\theta)$ is the full width at half-height and θ is the position of the related crystalline diffraction peak.

The results of the XRD investigations are listed in Tables 1 and 2.

TABLE 1. Experimental data for end-products obtained by mechanical alloying of Fe and Cu powders

Fe[a] (wt.%)	Fe[b] (wt.%)	Cr[c] (wt.%)	Δ(f.c.c.)[d] (%)	Φ(f.c.c.)[e] (nm)	Δ(b.c.c.)[d] (%)	Φ(b.c.c.)[e] (nm)	d[f] (10^{-1} nm)
Cu	12.7	0.8	+0.6	4–20	–	–	–
10	22.1±9	1.0	+0.4	6–18	−0.4	9	–
20	31.9±0.8	≤0.5	+0.5	6–13	–	–	2.08
30	40.0±4.0	≤1.2	+0.1	13–18	−0.6	18	–
40	60.7±1.2	≤2.5	+0.6	6–12	+0.1	18	2.07
50	62.1±4.6	≤1.5	+0.1	5–13	−0.5	7	2.04
60	64.5±0.3	≤1.8	+0.1	4–30	+0.4	3–11	2.02
65	66.8±0.3	≤1.3	+0.2	10–20	+0.8	4–8	1.99
70	73.0±1.8	≤0.7	–	–	+0.9	3–8	2.00
80	82.4±0.3	≤0.4	–	–	+0.5	4–9	2.02
90	90.5±0.4	≤0.4	–	–	+0.4	4–10	2.01
Fe	100	≤0.5	–	–	+0.4	4–8	–

[a]Initial composition; [b]end-product composition; [c]contamination by Cr of container; [d]relative change in f.c.c. and b.c.c. lattice parameters with respect to those of pure Cu and Fe phases respectively; [e]crystalline grain size of f.c.c. and b.c.c. phases; [f]amorphous halo position.

TABLE 2. Experimental data for end-products obtained by mechanical alloying of Fe and Cu powders with ethanol

Fe[a] (wt.%)	Fe[b] (wt.%)	Cr[c] (wt.%)	Δ(f.c.c.)[d] (%)	Φ(f.c.c.)[e] (nm)	Δ(b.c.c.)[d] (%)	Φ(b.c.c.)[e] (nm)	d[f] (10^{-1} nm)	Other phases
10	9.6±0.3	≤0.1	+0.3	10–20	–	–	2.07	Fe_3O_4
20	22.6±0.4	≤0.2	+0.5	8–20	–	–	2.08	Fe_3O_4
30	31.9±0.4	≤0.1	+0.5	20	–	–	2.07	Fe_3O_4
40	42.9±0.4	≤0.1	+0.6	10–13	−0.1 (?)	Traces	2.00	Fe_3C (?)+ Fe_3O_4
50	54.7±0.9	≤0.2	+0.7	10–13	0.0 (?)	Traces	2.05	Fe_3C+ Fe_3O_4 (?)
60	65.3±0.4	≤0.3	+1.0	10–13	0.0 (?)	Traces	2.07	Fe_3C
70	78.2±0.5	≤1.0	+0.1	4	0.0 (?)	Traces	1.86	Fe_3C+ Fe_3O_4 (?)
80	94.0±0.9	≤0.2	−1.8	4	+0.2	8	2.02	Fe_3C

[a–f]See footnote to Table 1 for explanation of column headings.

Some particular comments have to be noted concerning the interpretation of Tables 1 and 2.

2.3.1. Table 1

On the Fe-rich side of the phase diagram ($73 \leqslant Fe \leqslant 100$ wt.%) only the crystalline b.c.c. (Fe) phase has been detected in addition to the amorphous phase. In this domain the supersaturation leads to a linear increase in the lattice parameter as shown in Fig. 3(a). Such an observation supports the idea that a phase exhibiting a b.c.c. structure with a lattice parameter lower than the one corresponding to the pure Fe phase has not to be considered as being an (Fe) phase, but nothing more than an unknown b.c.c. phase. Thus, as observed in Table 1, the highest value of the end-product composition for which only the crystalline b.c.c. (Fe) phase has been detected is 62 wt.% Fe.

For the end-product compositions ranging from 65 to 67 wt.% Fe, both f.c.c. (Cu) and b.c.c. (Fe) added to an amorphous phase are detected.

2.3.2. Table 2

For the initial compositions with 40, 50, 60 and 70 wt.% Fe the diffraction peaks which may be attributed to the b.c.c. (Fe) phase appear to be very weak. Therefore the relative amount of the b.c.c. (Fe) phase is very low and (Fe) is denoted "?" and "traces" in the table. Furthermore, a linear dependence of the f.c.c. lattice parameter is observed for end-product compositions with up to about 65 wt.% Fe. In such a composition domain the only crystalline phase which has to be considered is f.c.c. (Cu) added to an amorphous phase.

For an end-product composition with 78 wt.% Fe the linear dependence is no longer observed. Such an MA product has to be considered as being a mixture

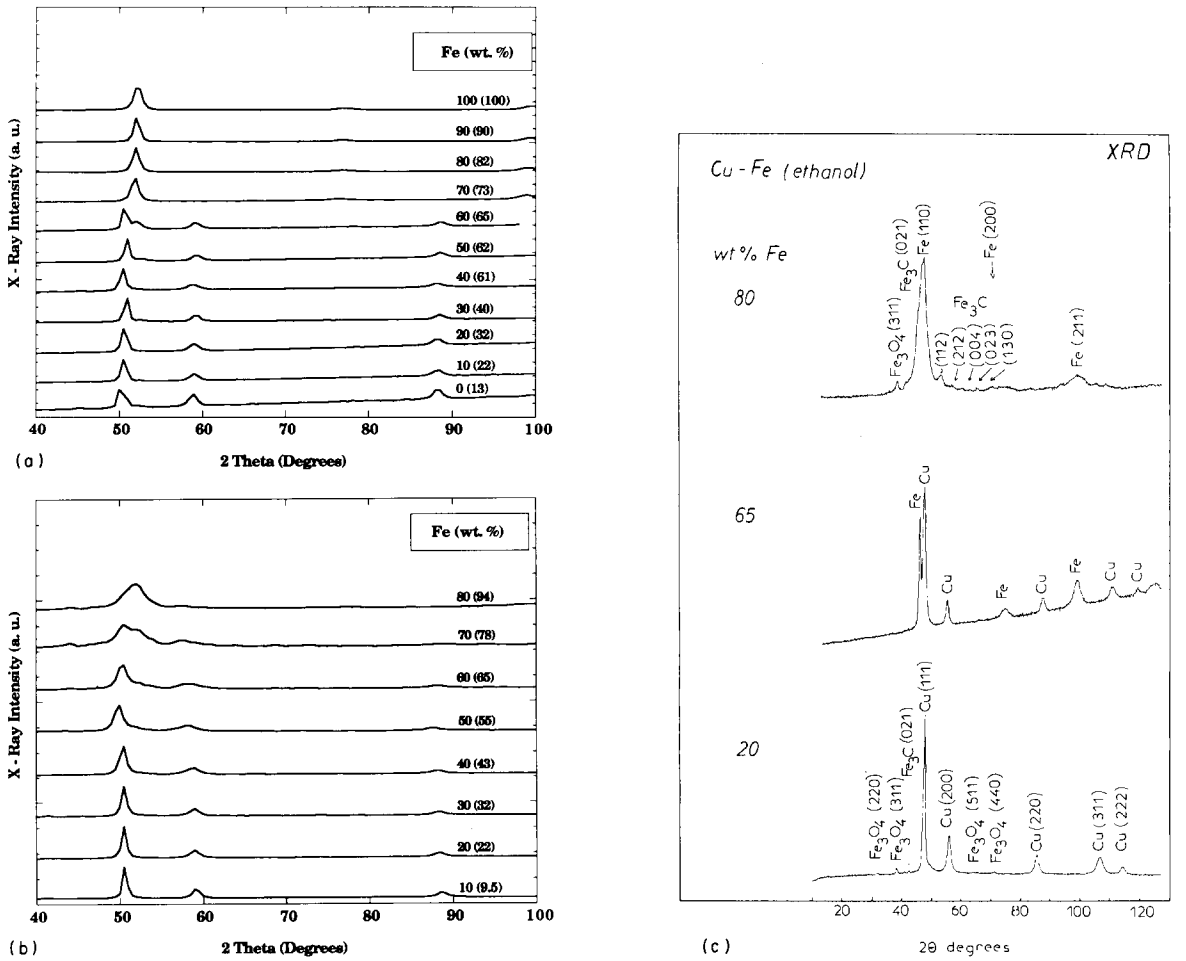

Fig. 2. X-Ray diffraction patterns obtained for all compositions: (a) MA without ethanol; (b), (c) MA with ethanol. The numbers in parentheses in (a) and (b) are the measured end-product compositions. The XRD peaks in (c) corresponding to the b.c.c. (Fe) and f.c.c. (Cu) major phases and to the Fe_3O_4 and Fe_3C minor phases are indicated (the compositions correspond to the initial ones).

of crystalline f.c.c. (Cu) and b.c.c. (Fe) phases added to an amorphous phase and Fe_3C and Fe_3O_4 phases.

For the initial composition with 80 wt.% Fe the relative change in the f.c.c. phase is −1.8%. Such a relative decrease leads to the interpretation that such a phase has not to be considered as being related to a (Cu) phase. Indeed, for the initial compositions with 10, 20 and 30 wt.% Fe, for which the end-product has been found to correspond only to a mixture of f.c.c. (Cu) and an amorphous phase (added to Fe_3O_4), the supersaturation results in an expansion of the f.c.c. lattice parameter. Such a comparison supports the idea that for the initial composition with 80 wt.% Fe only the crystalline b.c.c. (Fe) phase has to be considered (added to an amorphous phase and the Fe_3C phase).

2.4. *Thermal stability investigations*

The thermal analysis was carried out using a DSC-2C differential scanning calorimeter (Perkin–Elmer). A sample of about 50 mg was sealed in a copper capsule and heated from 50 to 725 °C under flowing pure argon. The DSC traces which are shown in Figs. 4(a) and 4(b) correspond to the first heating trace. Figures 4(a) and 4(b) correspond to the milling process without and with ethanol addition respectively. In Fig. 4(a), going from room temperature to higher temperatures, a very wide and intense exothermic peak contribution can be seen. Such an exothermic event has been attributed to the transition from the metastable supersaturated phases (crystalline and amorphous phases) to the stable elemental phase mixture.

For the initial compositions with 65 and 60 wt.% Fe this contribution is observed to be composed of two well-separated peaks. As mentioned above, the XRD investigation has revealed that for the initial compositions with 60–65 wt.% Fe the end-product is composed of a mixture of both b.c.c. and f.c.c. phases (added to an amorphous phase). Therefore the two well-separated exothermic peaks could be interpreted as corresponding to the transition of these metastable phases into crystalline ones.

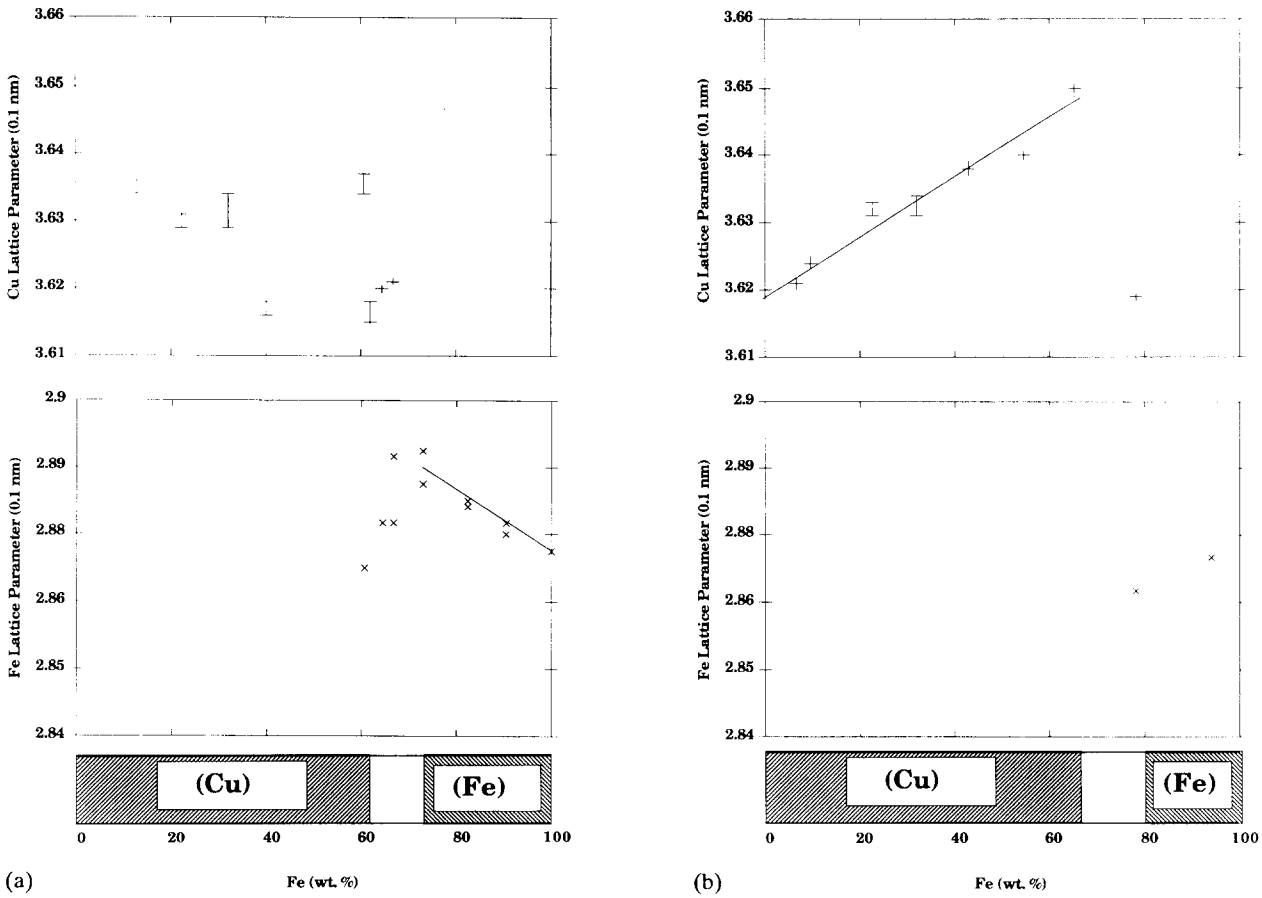

Fig. 3. Supersaturated f.c.c. (Cu) (top) and b.c.c. (Fe) (bottom) phase lattice parameters corresponding to (a) MA without solvent addition and (b) MA with ethanol addition ($a_{(\text{pure Cu})}=0.3615$ nm, $a_{(\text{pure Fe})}=0.2866$ nm).

2.5. Thermomagnetometric experiments

The Curie temperature has been determined using a modified microelectrobalance (type CI) equipped with a permanent magnet. The Curie temperatures of the powders obtained by the dry milling process as a function of the initial composition are shown in Fig. 5. The specimens were heated under flowing argon at a rate of 15 °C min^{-1}.

3. Discussion

3.1. Supersaturated phase formation

3.1.1. Crystalline phases

The reported experimental results describe the formation of the supersaturated f.c.c. and b.c.c. phases in the Cu–Fe system using a well-defined high energy planetary ball-milling apparatus. In the previously published works which reported on the supersaturated phase formation induced by mechanical alloying in the Cu–Fe system [13–16], no complete description of the milling machine was given which would help in the knowledge of the effective milling parameters such as the energy and the frequency of the shocks. In the present work the specially designed and realized high energy planetary milling machine allows electronic tachometer control of the effective rotation speed of the various moving parts of the apparatus.

In the case of the dry mechanical alloying process the X-ray diffraction investigations lead to the existence of three composition domains for which three end-product structures are observed (see Table 3): a crystalline f.c.c. (Cu) phase, a mixture of crystalline f.c.c. (Cu) and b.c.c. (Fe) phases and a crystalline b.c.c. (Fe) phase.

It has to be noted that for the Fe content in the composition domains ranging from 62 to 65 wt.% and from 67 to 73 wt.% no experimental results have been obtained (Table 1). This is the reason why the full composition domain dependence of the end-product structure has not been characterized.

It has to be noted also that in the case of the initial pure Cu powder a wide contamination by Fe is observed (about 13 wt.%). Such a contamination problem will be discussed later.

As observed in Fig. 3(a), the (Fe) lattice parameter (hereafter referred to as $a_{(\text{Fe})}$) exhibits a linear curve as a function of the Cu content (up to 27 wt.% Cu).

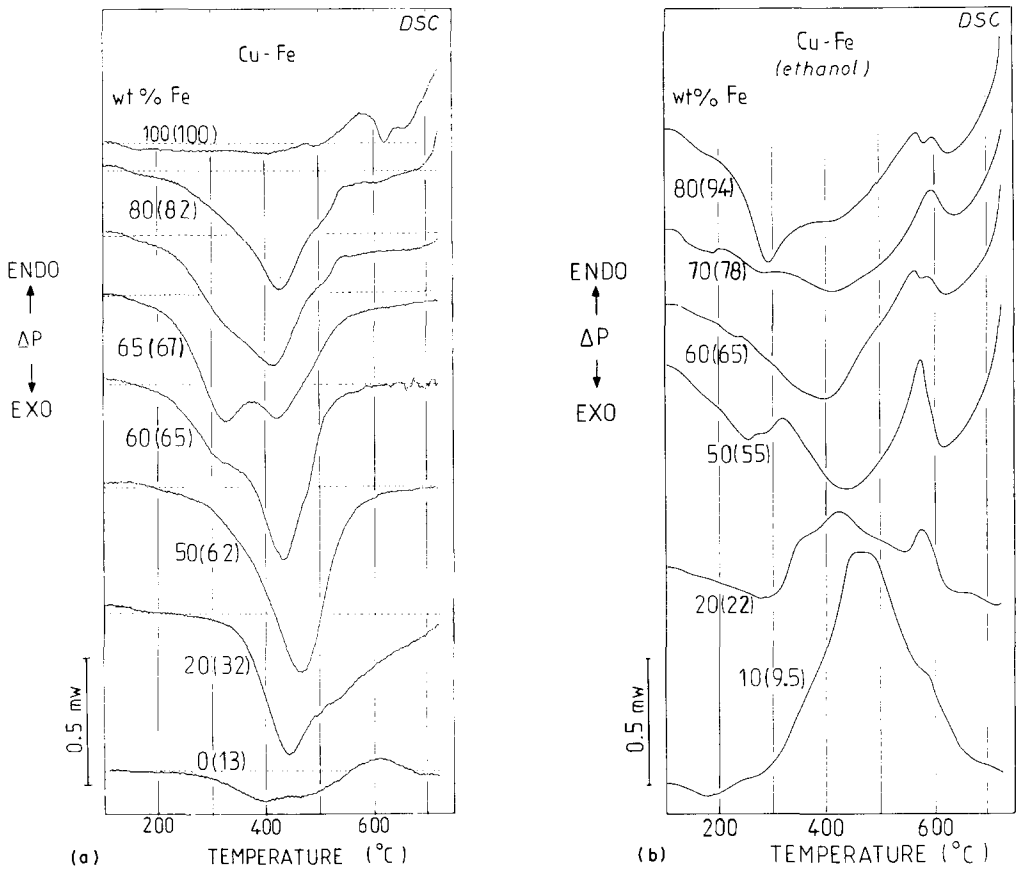

Fig. 4. DSC traces corresponding to MA end-product with respect to the initial Fe+Cu powder mixture composition: (a) MA without ethanol; (b) MA with ethanol. The numbers in parentheses are the measured end-product compositions.

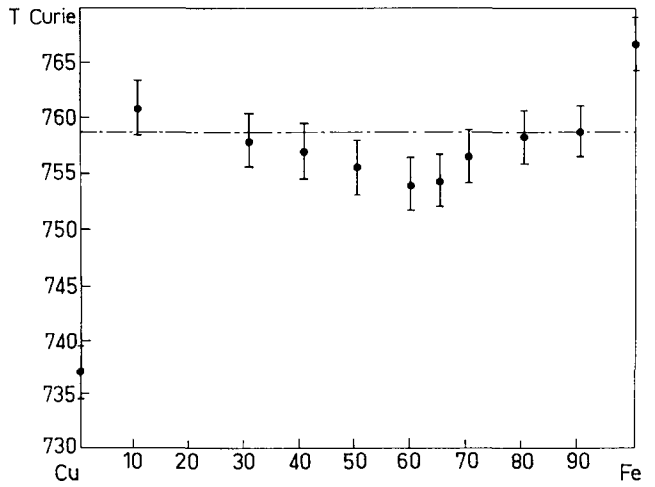

Fig. 5. Curie temperatures of the powders obtained by the dry milling process as a function of the initial composition.

Such a Vegard-type law has been calculated to correspond to the expression

$$a_{(Fe)} = 0.2877 + 1.626 \times 10^{-5}\, C_{Cu}$$

where $a_{(Fe)}$ is expressed in nanometres and C_{Cu} (wt.%) is the end-product Cu content.

TABLE 3. Supersaturated (Cu) and (Fe) phase domains (expressed as end-product composition) as a function of the mechanical alloying process (without and with ethanol)

Phase	Without ethanol	With ethanol
F.c.c. (Cu)	0–62 wt.% Fe	0–65 wt.% Fe
F.c.c. (Cu)+b.c.c. (Fe)	65–67 wt.% Fe	78 wt.% Fe
B.c.c. (Fe)	0–27 wt.% Cu	0–20 wt.% Cu

3.1.2. *Amorphous phases*

As seen in Tables 1 and 2, the XRD investigations reveal the presence of an amorphous phase by the detection of a diffuse and wide halo. The position of this halo has been reported in the tables. No significant change in the halo position is found. It is noteworthy that the position of the amorphous halo is superimposed on the [110] peak of the (Fe) phase.

3.2. *Ethanol effect*

The effects of ethanol addition to the initial mixture of Fe and Cu powders are seen clearly in Tables 1 and 2 and have been summarized in Table 3. Various influences are observed.

3.2.1. Expansion of the solubility limit

Expansion of the concentration domain of the (Cu) phase. As mentioned above, considering the fact that the Vegard-type law of the (Cu) lattice parameter (hereafter referred to as $a_{(Cu)}$) extends up to 65.3 wt.% Fe, the expansion of the (Cu) domain has to be considered as being 65%. In such an Fe content domain the expression corresponding to the (Cu) lattice parameter is

$$a_{(Cu)} = 0.3619 + 4.3448 \times 10^{-5}\, C_{Fe}$$

where $a_{(Cu)}$ is expressed in nanometres and C_{Fe} (wt.%) is the end-product Fe content.

As mentioned above, a slight difference is observed between the two supersaturated (Cu) phase domains obtained without and with ethanol addition. Nevertheless, the fact that the (Cu) lattice parameter exhibits a Vegard-type law in the case of wet milling supports the idea that such a wet process leads to a better homogenization of the end-product in terms of the (Cu) phase composition than in the case of dry milling.

Expansion of the concentration domain of the (Fe) phase. Considering Figs. 3(a) and 3(b), the b.c.c. (Fe) composition domain depends on the milling conditions: with ethanol the supersaturation has been observed to reach 20 wt.% Cu, but without ethanol a higher supersaturation of 27 wt.% Cu has been obtained. This difference is significant.

3.2.2. Oxide and carbide phase formation

The second effect is the formation of the Fe oxide and Fe carbide phases. As shown by Fig. 2(c), minor XRD peaks are observed on the XRD patterns corresponding to milling using ethanol. As observed in Table 2, the presence of both phases depends on the end-product Fe content as follows:

Fe_3O_4	$0 \leqslant Fe \leqslant 32$ wt.%
$Fe_3O_4 + Fe_3C$	$32 < Fe \leqslant 78$ wt.%
Fe_3C	$78 < Fe \leqslant 94$ wt.%

3.2.3. Homogeneous end-product

Another aspect of the solvent addition is the fact that after such a long milling duration it is possible to recover the total amount of the initial powder mixture. In other words, the sticking of powder on the balls and/or on the walls is nearly eliminated by solvent addition.

Such a decrease in the so-called "powder to balls and walls" sticking leads to a better homogenization of the milled powder content, *i.e.* the end-product composition is close to that of the initial mixture. As seen in Tables 1 and 2, this positive effect of solvent addition is particularly evident for the Cu-rich initial compositions.

However, on the Fe-rich side it seems that the addition of a solvent has resulted in Fe enrichment of the end-product powder in comparison with the initial composition. To our knowledge this is the first time that such an effect has been reported, though up to now no explanation has been found.

3.2.4. Lower container contamination

Furthermore, owing to the decrease in the sticking interaction between the milled powder and the balls and walls, there is a decrease in Cr contamination (coming from the container and the balls) of the powder mixture which has been obtained starting with an initial solvent addition.

3.3. Magnetometric experiments

The results presented in Fig. 5 are consistent with the decomposition of the supersaturated phases into nearly pure f.c.c. Cu and b.c.c. Fe, because the Curie temperature remains almost constant and is close to the equilibrium value of (Fe). In other words, the metastable f.c.c. and b.c.c. phases are destabilized before reaching their Curie temperature. This experimental result is in good agreement with the previously published results of Yavari *et al.* [15] and with the DSC results presented in this work and developed in more detail in ref. 21.

4. Conclusions

On the basis of the present experimental studies (X-ray diffraction characterizations and thermal stability investigations), far-from-equilibrium supersaturated phase formation induced by mechanical alloying has been observed in the Cu–Fe system.

On the Cu-rich side of the MA Cu–Fe phase diagram the addition of a solvent (here ethanol) to the initial powder mixture leads to an expansion of the supersaturated f.c.c. (Cu) phase domain (up to 65 wt.% Fe) with the f.c.c. lattice parameter exhibiting a Vegard-type law dependence. Such a Vegard-type law is not observed in the case of the dry MA process, the supersaturated f.c.c. (Cu) phase domain expanding up to 62 wt.% Fe.

On the Fe-rich side of the MA Cu–Fe phase diagram no benefit is gained by ethanol addition. In fact, the dry MA process appears to be the best one, resulting in the formation of a well-defined supersaturated b.c.c. (Fe) phase (up to 27 wt.% Cu) with the lattice parameter following a Vegard-type law. Such a linear dependence is not observed in the case of the milling process performed with ethanol. In the latter case the supersaturated b.c.c. (Fe) phase is restricted to 0–20 wt.% Cu.

Such an ethanol addition has been found to introduce some contamination by Fe_3O_4 and Fe_3C phases on the Cu-rich and Fe-rich sides of the Cu–Fe composition range respectively. This could be an advantage for hardening the sintered powder.

Further investigations are now being performed in order to analyse the kinetics of the supersaturated phase formation and to study the effect of the milling conditions (*i.e.* the energy and the frequency of the shocks) on the kinetics.

Acknowledgment

The authors thank the workshop staff (CECM/CNRS) for their help in the design and realization of the planetary milling machine.

References

1 A. E. Yermakov, E. E. Yurchikov and V. A. Barinov, *Fiz. Met. Metalloved., 52* (1981) 1184.
2 C. C. Koch, O. B. Cavin, C. G. McKamey and J. O. Scarbrough, *Appl. Phys. Lett., 43* (11)(1983) 1017.
3 A. W. Weeber and H. Bakker, *Z. Chem. Phys. N.F., 157* (1988) 221.
4 E. Gaffet and M. Harmelin, *J. Phys. (Paris), Colloq. C4, Suppl. 14, 51* (1990) 139.
5 C. H. Lee, T. Fukunaga and U. Mizutani, *Mater. Sci. Eng. A, 134* (1991) 1334.
6 T. Fukunaga, M. Mori, K. Inou and U. Mizutani, *Mater. Sci. Eng. A, 134* (1991) 863.
7 E. Gaffet, C. Louison, M. Harmelin and F. Faudot, *Mater. Sci. Eng. A, 134* (1991) 1380.
8 E. Gaffet and M. Harmelin, *J. Less-Common Met., 157* (1990) 201.
9 E. Gaffet, *Mater. Sci. Eng. A, 136* (1991) 161.
10 E. Gaffet, F. Faudot and M. Harmelin, *Mater. Sci. Eng. A, 149* (1991) 85.
11 E. Gaffet and J.-P. Gaspard, *J. Phys. (Paris), Colloq. C4, Suppl. 14, 51* (1990) 139.
12 D. G. Morris and M. A. Morris, *Scr. Metall. Mater., 24* (1990) 1701.
13 P. H. Shingu, K. N. Ishihara, K. Uenishi, J. Kuyama, B. Huang and S. Nasu, in A. H. Clauer and J. J. deBarbadillo (eds.), *Proc. Solid State Powder Processing*, Minerals, Metals and Materials Society, Indianapolis, IN, 1989, p. 21.
14 K. Uenishi, K. F. Kobayashi, S. Nasu, H. Hatano, K. N. Ishihara and P. H. Shingu, *Z. Metallk., 83* (1992) 132.
15 A. R. Yavari, P. J. Desré and T. Benameur, *Phys. Rev. Lett., 68* (1992) 2235.
16 A. R. Yavari and P. J. Desré, in A. R. Yavari (ed.), *Proc. Ordering and Disordering in Alloys,* Elsevier, London, 1992, p. 414.
17 E. Gaffet and L. Yousfi, *Mater. Sci. Forum, 88–90* (1992) 51.
18 E. Gaffet, *Mater. Sci. Eng. A, 132* (1991) 181.
19 E. Gaffet, N. Merk, G. Martin and J. Bigot, *Proc. DGM Conf. on New Materials by Mechanical Alloying Techniques, Hirsau, October 1988,* Deutsche Gesellschaft für Metallkunde, Darmstadt, 1989, pp. 95–100.
20 A. Antoniadis, J. Berruyer and A. Filhol, *Internal Rep. 87AN22T*, 1988, (Laue Langevin Institute, Grenoble).
21 F. Faudot, E. Gaffet and M. Harmelin, *J. Mater. Sci.*, in press.